Biogeosciences Discuss., 8, 10617–10644, 2011
www.biogeosciences-discuss.net/8/10617/2011/
doi:10.5194/bgd-8-10617-2011

Biogeosciences Discussions

Impact of rapid sea-ice reduction in the Arctic Ocean on the rate of ocean acidification

A. Yamamoto[1,2], **M. Kawamiya**[1], **A. Ishida**[1,3], **Y. Yamanaka**[1,2], **and S. Watanabe**[1]

[1]Japan Agency for Marine-Earth Science and Technology, Yokohama, Japan
[2]Graduate school of Environmental Science, Hokkaido University, Sapporo, Japan
[3]Department of Social Environment, Fuji Tokoha University, Fuji, Japan

Received: 7 October 2011 – Accepted: 21 October 2011 – Published: 28 October 2011

Correspondence to: A. Yamamoto (akitomo@jamstec.go.jp)

Published by Copernicus Publications on behalf of the European Geosciences Union.

Abstract

The largest pH decline and widespread undersaturation with respect to aragonite in this century due to uptake of anthropogenic carbon dioxide in the Arctic Ocean have been projected. The reductions in pH and aragonite saturation state have been caused primarily by an increase in the concentration of atmospheric carbon dioxide. However, in a previous study, simulations with and without warming showed that these reductions in the Arctic Ocean also advances due to the melting of sea ice caused by global warming. Therefore, future projections of pH and aragonite saturation in the Arctic Ocean will be affected by how rapidly the reduction in sea ice occurs. In this study, the impact of sea-ice reduction rate on projected pH and aragonite saturation state in the Arctic surface waters was investigated. Reductions in pH and aragonite saturation were calculated from the outputs of two versions of an earth system model (ESM) with different sea-ice reduction rates under similar CO_2 emission scenarios. The newer model version projects that Arctic summer ice-free condition will be achieved by the year 2040, and the older version predicts ice-free condition by 2090. The Arctic surface water was projected to be undersaturated with respect to aragonite in the annual mean when atmospheric CO_2 concentration reached 480 (550) ppm in year 2040 (2048) in new (old) version. At an atmospheric CO_2 concentration of 520 ppm, the maximum differences in pH and aragonite saturation state between the two versions were 0.08 and 0.15, respectively. The analysis showed that the decreases in pH and aragonite saturation state due to rapid sea-ice reduction were caused by increases in both CO_2 uptake and freshwater input. Thus, the reductions in pH and aragonite saturation state in the Arctic surface waters are significantly affected by the difference in future projections for sea-ice reduction rate. The critical CO_2 concentration, at which the Arctic surface waters become undersaturated with respect to aragonite on annual mean bias, would be lower by 70 ppm in the version with the rapid sea-ice reduction.

BGD

8, 10617–10644, 2011

1 Introduction

The emission of large amounts of anthropogenic carbon dioxide (CO_2) has increased global atmospheric CO_2 concentration from a preindustrial value of 280 ppm to 384 ppm in 2007, and is contributing to global warming (IPCC, 2007). Rising atmospheric CO_2 and global warming are tempered by oceanic uptake, which absorbs nearly one-third of anthropogenic CO_2 released to the atmosphere (Sabine et al., 2004). However, anthropogenic CO_2 penetration into the ocean increases hydrogen ion concentration and causes a reduction in pH, a process known as ocean acidification. The average surface ocean pH has already decreased by about 0.1 (from a pH of 8.2 to 8.1) since the 1700s due to absorption of anthropogenic CO_2 (Royal Society, 2005), and a previous modeling study suggested that an additional decrease of 0.3–0.4 will occur when atmospheric CO_2 concentration reaches 800 ppm by the year 2100 (Orr et al., 2005). This reduction in ocean pH has some direct effects on many marine organisms (Seibel and Walsh, 2001; Ishimatsu et al., 2005).

Carbonate ion (CO_3^{2-}) concentrations and the saturation state (Ω) of calcium carbonate ($CaCO_3$) minerals such as calcite and aragonite also are decreased due to dissolution of CO_2 into the ocean. Carbonate ions are required by marine calcifying organisms such as plankton, shellfish, coral, and fish to produce $CaCO_3$ shells and skeletons. Shell and skeleton formation generally occurs in supersaturated seawater ($\Omega > 1.0$) and dissolution occurs in undersaturated seawater ($\Omega < 1.0$). Thus, $CaCO_3$ saturation state is a key variable for assessing the biological impacts of ocean acidification. In surface waters, Ω is lower in cold high-latitude oceans than in tropical and temperate oceans because of increased CO_2 solubility, the sensitivity of acid-base dissociation coefficients at cold temperatures, and ocean mixing patterns. Although surface waters in high-latitude oceans today are generally supersaturated with respect to aragonite (aragonite is more soluble than calcite), recent studies have reported undersaturated seawater in the Canada Basin of the Arctic Ocean (Yamamoto-Kawai et al., 2009; Bates et al., 2009). From the modeling projections, small regions of surface

BGD
8, 10617–10644, 2011

water in the Arctic Ocean may already be undersaturated with respect to aragonite (Gangstø et al., 2008) or will become undersaturated within a decade under the A2 Scenario of the Special Report on Emissions Scenarios (SRES-A2) (Steinacher et al., 2009). After that, undersaturation will begin to occur in the Southern Ocean by 2030 (McNeil and Matear, 2008), and the North Pacific by 2100 under IS92a scenario, which is similar to the SRES-A2 scenario (Orr et al., 2005). Therefore, understanding the aragonite saturation state (Ω_{arag}) decreases in the Arctic Ocean, which is projected to be the first ocean to experience undersaturation, is important for avoiding the risk of large changes in marine ecosystems.

Future surface pH and Ω_{arag} value closely track changes in atmospheric CO_2 because the equilibrium of dissolved inorganic carbon follows well-established chemistry in seawater and the effect of climate change is relatively small (Orr et al., 2005; Zeebe et al., 2008). Steinacher et al. (2009) suggested that sea-ice reduction in the Arctic Ocean reduces pH and Ω_{arag} by comparing the simulations with and without warming. This is because, the increases in CO_2 uptake by air-sea gas exchange due to the disappearance of sea-ice cover and freshwater input from increased precipitation, river runoff, and ice melt decrease pH and Ω_{arag} in the Arctic Ocean. Thus, projections of pH and Ω_{arag} values for the Arctic Ocean are affected by sea-ice reduction due to climate change. In most model projections adopted for IPCC AR4, summer sea ice in the Arctic Ocean will still remain until 2100, and only a few models predict sea-ice free Arctic in September by the end of the twenty-first century. However the observed recent Arctic sea-ice loss has been more rapid than projected in these models adopted for IPCC AR4 (Stroeve et al., 2007). Wang and Overland (2009) predicted sea-ice free Arctic in September by the year 2037, by correcting biases in six IPCC AR4 models based on the extent of the observed 2007 September sea ice as a starting point. The rate of ocean acidification in the Arctic Ocean, if projected with a model that gives a summer sea-ice free condition within 30 years, would be faster than that under the condition of summer sea ice remaining until the end of the twenty-first century.

BGD
8, 10617–10644, 2011

In this study, the relation between rates of sea-ice reduction and surface ocean acidification was investigated by comparing the rates of ocean acidification from outputs of two versions of an earth system model (ESM) in which different sea-ice reduction rates are projected under similar CO_2 emission scenarios. One ESM projects summer ice-free condition by the year 2040 under the Representative Concentration Pathways 8.5 (RCP8.5) scenario (Moss et al., 2010), and the other ESM by 2090 under the SRES A2 scenario. First, pH and Ω_{arag} projected for both models are compared with the observed value, and model biases are calculated. Then, we investigate the difference in fundamental variables between two versions of ESM due to rapid sea-ice reduction. The surface pH and Ω_{arag} modified by removing model biases were compared, and the areal fraction occupied by undersaturated surface water that increases with atmospheric CO_2 concentration for our two versions of ESM was calculated. This was an estimate of the impact of sea-ice reduction on the rate of ocean acidification in the Arctic Ocean. The mechanisms promoting ocean acidification due to rapid sea-ice reduction, and the difference in behavior between pH and Ω_{arag} under high atmospheric CO_2 concentrations are discussed. The change of the seasonal cycle due to sea-ice reduction also was discussed.

2 Methods

2.1 Models and experiments

The two versions of ESM used were MIROC-ESM (Watanabe et al., 2011) and its prototype version (Kawamiya et al., 2005). Hereafter, these two versions are designated the "new" version (NV) and "old" version (OV), respectively. OV was adopted for the Coupled Climate-Carbon Cycle Model Intercomparison Project (C^4MIP) with a name "FRCGC" (Friedlingstein et al., 2006); it made a significant contribution to IPCC AR4. NV was developed for IPCC AR5. Two versions are based on the physical climate system model MIROC in which atmosphere, ocean, sea ice, land surface components,

BGD
8, 10617–10644, 2011

and river routine are coupled by a flux coupler without flux adjustments (K-1 Model Developers, 2004). The atmospheric model used in OV (NV) has a horizontal resolution of T42, approximately equivalent to a 2.8° grid size with 20 (80) vertical levels. The ocean and sea-ice model in both versions is the same. The ocean model has a zonal resolution of 1.4° and a spatially varying meridional resolution that is about 0.56° at latitudes lower than 8° and 1.4° at latitudes higher than 65° and changes smoothly in between. The vertical coordinate is a hybrid of sigma-z, resolving 44 levels in total: 8 sigma-layers near the surface, and 35 z-layers beneath, plus one boundary layer. The sea ice is based on a two-category thickness representation, zero-layer thermodynamics (Semtner, 1976), and dynamics using elastic-viscous-plastic rheology (Hunke and Dukowicz, 1997).

On the basis of MIROC, NV incorporates the terrestrial ecosystem model SEIB-DGVM (Sato et al., 2007) dealing with dynamic vegetation, and OV has Sim-CYCLE (Ito and Oikawa, 2002), which is a terrestrial carbon model with fixed vegetation. Ocean biological and chemical processes in both versions are represented by a four-compartment model consisting of nutrients, phytoplankton, zooplankton, and detritus (Oschlies and Garcon, 1999; Oschlies, 2001). This NPZD type ocean ecosystem model is enough to resolve the seasonal excursion of oceanic biological activities on a basin scale (Kawamiya et al., 2000). In addition, a series of inorganic carbon reactions have been introduced following recommendations by the Ocean Carbon Pattern Model Intercomparison Project (OCMIP) (Orr et al., 1999).

We used model outputs of OV conducted by Yoshikawa et al. (2008) under SRES A2 (Fig. 1a). The results of MIROC spin-up conducted by the K-1 Model Developers (2004) were provided for the physical climate system. The spin-up run for the carbon cycle component in OV was conducted by running the integrated model for 250 years, starting with the initial conditions based on climatologic data sets until globally integrated net CO_2 fluxes at land and sea surfaces vanished. Historical simulation was performed for the years from 1850 to 1999 using observed anthropogenic fossil fuel emission (Marland et al., 2005) and CO_2 emission was given based on SRES A2 for

BGD
8, 10617–10644, 2011

2000–2100. The spin-up run and historical simulation using a set of external forcings recommended by the Coupled Model Intercomparison Project phase-5 (CMIP5) throughout 1850–2005 in NV were conducted by Watanabe et al. (2011). The RCP8.5 was given for 2006–2100 in NV. It may be noteworthy that atmospheric CO_2 concentration in OV was predicted by the carbon-cycle components with the given CO_2 emissions, while it was provided as input data for NV following the CMIP5 protocol. There was little difference in atmospheric CO_2 concentration between two versions, with a maximum difference of 60 ppm in 2100.

2.2 Carbonate calculation and target area

Model outputs of seawater temperature (T), salinity (S), alkalinity (Alk), and dissolved inorganic carbon (DIC), and observational values of phosphate (PO_4^{3-}) and silicate ($Si(OH)_4$) were used for deriving diagnosis on carbonate chemistry. These two observational datasets were used from the World Ocean Atlas 2005 (Locarnini et al., 2006) because these two parameters are not calculated in our ESM. However, the influence of treatments such as PO_4^{3-} and $Si(OH)_4$ on pH and Ω_{arag} are very small. To compute pH and carbonate ion values, the parameters and the chemistry routine from the OCMIP-3 project (http://ocmip5.ipsl.jussieu.fr/OCMIP) were used. Surface $CaCO_3$ solubility product was calculated based on Mucci (1983) and the pressure effect based on Millero (1995). For comparison with projected pH and Ω_{arag}, observed values were calculated using OCMIP chemistry routine and the data of T, S, Alk, DIC, PO_4^{3-}, and $Si(OH)_4$ from the Arctic Ocean Expedition 1991 (ODEN-91, cruise 77DN1991072), Arctic Ocean Section 1994 (AOS-94, cruise 18SN19940726), and the Arctic Climate System Study 1996 (ARCSYS-96, cruise 06AQ19960712). These data are available from the CARINA database (http://cdiac.ornl.gov/oceans/CARINA/Carina_table.html). The pH and Ω_{arag} values in more recent periods were calculated using observed T, S, Alk and DIC in the Joint Ocean Ice Study (JOIS) 2008 (Yamamoto-Kawai et al., 2009) and August PO_4^{3-} and $Si(OH)_4$ concentrations of the World Ocean Atlas 2005.

BGD
8, 10617–10644, 2011

The target area of Arctic Ocean defined here is north of 65° N, except for the Labrador Sea and Greenland, Iceland, Norwegian, and Barents Seas (<80° N and 35° W–60° E) where sea ice does not exist in OV or NV. Those areas were excluded from the analysis because the present study focuses on the effect of sea-ice reduction on ocean acidification.

3 Results

3.1 Comparison of pH and aragonite saturation between model and observation

The Ω_{arag} and pH in the top 200 m of the Arctic Ocean predicted in the two model versions were compared with observed values calculated from ODEN-91, AOS-94, ARCSYS-96, and JOIS 08 for the same place and time (Fig. 2). A comparison of the two model versions with the 1990s observations of ODEN-91, AOS-94, and ARCSYS-96 reveals that OV (NV) tends to underestimate Ω_{arag} by 0.21 (0.23) at the surface, although the underestimation decreases significantly toward a depth of about 45 m. The projected Ω_{arag} below 45 m is overestimated by up to 0.3 (0.4). In comparison with JOIS 08, OV (NV) tends to overestimate (underestimate) Ω_{arag} by 0.1 (0.07) at the surface. Below 60 m, the projected Ω_{arag} is greatly overestimated by up to 0.73 (0.89). The difference in modern sea-ice extent projected in the two versions does not make a significant difference in Ω_{arag} in the Arctic surface waters. The projected average surface pH in the Arctic Ocean for both versions is about 0.02 lower than the observed values.

3.2 Comparison of physical and carbon-system variables between the two model versions

The Arctic sea-ice extent projected by the two model versions was compared with that based on the observational dataset of the Hadley Center sea-ice concentration analysis

BGD
8, 10617–10644, 2011

(HadISST) (Fig. 1). The sea ice extent is defined here as the total area of grid cells with a sea ice concentration greater than 15 %, as adopted by Wang and Overland (2009). In September, observed sea-ice extent was 9.4×10^6 km^2 in 1950, which rapidly decreased to 4.6×10^6 km^2 by 2007. NV reproduces the observed decrease well from 1970 and projects ice-free condition in September by 2040. In contrast, OV overestimates sea-ice extent in September by up to 80 % and projects ice-free condition by 2090. The September ice-free condition by 2040 projected in NV is consistent with recent studies (Holland et al., 2006; Stroeve et al., 2007; Wang and Overland, 2009). The projected summer sea-ice reduction for both versions are more rapid than in the Climate System Model CSM1.4-carbon of the US National Center for Atmospheric Research, which was used by Steinacher et al. (2009) for analyzing Arctic acidification, in which the sea-ice extent in September is 2.3×10^6 km^2 in 2100 under the SRES A2 scenario. The rapid sea-ice reduction in NV results in ice-free condition lasting more than 6 months and changing the Arctic Ocean into a seasonal sea-ice zone after 2080, whereas that condition lasts only 2 months in 2100 for OV. In March, the observed sea-ice extent is 15.6×10^6 km^2 in 1950, and gradually decreases to 14.5×10^6 km^2 by 2007. NV (OV) underestimates (overestimates) sea-ice extent in March, however, the differences in March sea-ice extent between the two model versions and the direct observations are within 10 %. The sea-ice extent in March projected by NV (OV) remains greater than 20 % (70 %) of the observed present-day value until 2100.

Disappearance of sea ice enhances CO_2 uptake through changes in air-sea gas exchange and marine biological productivity due to an increase in sea surface temperature and light penetration. Increased freshwater input due to melting of sea ice dilutes salinity, total CO_2 and alkalinity. Thus, NV with rapid sea-ice reduction yields an earlier and greater increase in seawater temperature, CO_2 uptake, and marine biological productivity, along with decreases in salinity and alkalinity in the Arctic surface waters (Fig. 3). The decrease in DIC in NV after 2040 is caused by rapid sea-ice reduction, which leads to a decrease in DIC due to freshwater input and biological processes that counteract the DIC increase due to CO_2 uptake. DIC in OV remains almost unchanged

BGD
8, 10617–10644, 2011

up to 2100, because an increase in DIC due to CO_2 uptake is offset by a decrease in DIC due to freshwater input and biological processes.

Furthermore, the partial pressure of carbon dioxide (pCO_2) in the Arctic surface waters is lower than in the atmosphere, partly because sea ice limits air-sea gas exchange. September pCO_2 values in the Arctic surface waters reproduced by the two model versions is about 290 µatm in the 1990s (atmospheric $CO_2 \approx 360$ ppm), which is consistent with the observations by Jutterström and Anderson (2010), who reported a typical value less than 300 µatm. A reduction in sea ice enables the ocean to come closer to equilibrium with the atmosphere. Therefore, when the atmospheric CO_2 exceeds 340 ppm, the rapid increase in CO_2 uptake due to rapid summer sea-ice reduction raises seawater pCO_2 in NV more than in OV under the same atmospheric CO_2 concentration. The maximum difference in annual mean surface water pCO_2 between the two model versions is 80 µatm at 520 ppm (year ≈ 2045, which is a few years after the difference in summer sea-ice extent reaches a maximum). After that, the increase in pCO_2 in OV by CO_2 uptake due to summer sea-ice reduction is greater than that in NV due to winter sea-ice reduction. Thus, the difference in pCO_2 between two versions decreased to 50 µatm. Simulated saturation fractions, defined here as oceanic pCO_2 values in terms of fraction of the saturation value with respect to atmospheric CO_2 concentration, are less than 80 % before 2000. The saturation fractions in both versions increased to 90 % near the time when the Arctic Sea becomes ice-free in summer, and then slowly approach 100 %.

3.3 Comparison of pH and aragonite saturation between two versions

In this section, we compare the bias-corrected annual mean Ω_{arag} and pH averaged in the Arctic surface waters between our two model versions. The averaged model bias was applied to all model grids of the Arctic surface water, since focus is on the difference in changes of Ω_{arag} resulting from sea-ice reduction averaged across the Arctic Ocean in the two model versions. The model bias subtracted from model projections is not Ω_{arag} but T, S, DIC and Alk because these four parameters are conserved

BGD
8, 10617–10644, 2011

quantities. The modified DIC ($DIC_{(mod.)}$) after removing model bias is described by $DIC_{(mod.)} = DIC_{(model)} - \overline{DIC_{(corr.)} - DIC_{(obs.)}}$, where $DIC_{(model.)}$ is the value projected in the respective version. $\overline{DIC_{(corr.)} - DIC_{(obs.)}}$ is the average model bias of DIC between the observed values ($DIC_{(obs.)}$) from ODEN-91, AOS-94, ARCSYS-96, and JOIS 08, and the model values ($DIC_{(corr.)}$) corresponding to the place and time of the observations. Seawater temperature, salinity and alkalinity are corrected in the same manner. The bias-corrected Ω_{arag} was calculated using these corrected parameters. The calculated model bias of Ω_{arag} in 1995 is −0.2 (−0.23) in OV (NV) at the surface. There is little difference in projected annual mean pH and Ω_{arag} averaged in the Arctic surface water between the two versions below an atmospheric CO_2 concentration of 360 ppm (Fig. 4). Values of these two variables for NV are less than those for OV at CO_2 concentrations greater than 360 ppm, beyond which rapid summer sea-ice reduction starts in NV. Annual mean Ω_{arag} in OV (NV) becomes less than one at 550 (480) ppm at year 2048 (2040). The maximum differences in pH and Ω_{arag} between the two versions are 0.08 and 0.15, respectively, at 520 ppm when the difference in seawater pCO_2 for the two versions reaches a maximum. These results indicate that the reductions in pH and Ω_{arag} in the Arctic surface waters are significantly accelerated by rapid sea-ice reduction. Differences in pH and Ω_{arag} between the two model versions decrease at atmospheric CO_2 concentrations greater than 520 ppm due to the decrease in pCO_2 difference from 80 µatm to 50 µatm. The difference in pH decreases to 0.05 and remains above 600 ppm whereas that of Ω_{arag} approaches to 0 despite a difference of 50 µatm in pCO_2. We discuss what causes these different responses of pH and Ω_{arag} in Sect. 4.2.

The areal fraction of undersaturated surface seawater with respect to aragonite in the Arctic Ocean for the two model versions are calculated as an index for indentifying atmospheric CO_2 concentration beyond which acidification may cause serious consequences. This was done to help establish firm criteria for atmospheric CO_2 concentrations that prevent widespread aragonite dissolution (Fig. 5). The bias-corrected Ω_{arag} also is used for this calculation. About 10 % of the surface waters in OV (NV)

BGD
8, 10617–10644, 2011

is projected to become undersaturated with respect to aragonite in at least one month of the years when atmospheric CO_2 reaches 406 (394) ppm. At CO_2 levels of 438 (425) ppm, 10 % of the surface area in OV (NV) is projected to become undersaturated throughout the year. More than 50 % of the surface area becomes undersaturated at 537 (493) ppm, and the entire surface area becomes undersaturated year around at 683 (672) ppm. The extension of underasaturated surface seawater also is influenced by sea-ice reduction rate. Adopting a criterion of year-round undersaturated seawater in 10 % of the surface area in the Arctic Ocean (Steinacher et al., 2009) and the rapid sea-ice reduction as projected by NV, the atmospheric CO_2 concentration should not exceed 425 ppm.

4 Discussion

4.1 Which mechanisms reduce pH and Ω_{arag} due to rapid sea-ice reduction?

The factors affecting pH and Ω_{arag} are seawater temperature (T), salinity (S), CO_2 uptake by gas exchange with the atmosphere (Gas), freshwater input (Fw), biology (Bio) and transport of carbon by lateral and vertical seawater exchange (Trans). To quantify the effects of these mechanisms on the reductions in pH and Ω_{arag} in the top 50 m of the Arctic Ocean due to rapid sea-ice reduction, we divide the changes in pH and Ω_{arag} into components corresponding to the six mechanisms for each model result. Ω_{arag} (pH) is represented by:

$$\Omega_{arag} = F(T, S, \mathrm{DIC}, \mathrm{Alk}), \quad (1)$$

where F is a function describing the relation between Ω_{arag} and the four factors. Gas exchange, freshwater input, biology and carbon transport affect pH and Ω_{arag} through changes in alkalinity and/or DIC. The annual response of Ω_{arag} (pH) can be expressed

BGD
8, 10617–10644, 2011

by the following equation:

$$\Delta\Omega_{\mathrm{arag}} = \frac{\partial\Omega_{\mathrm{arag}}}{\partial T}\Delta T + \frac{\partial\Omega_{\mathrm{arag}}}{\partial S}\Delta S + \frac{\partial\Omega_{\mathrm{arag}}}{\partial \mathrm{DIC}}\Delta\mathrm{DIC}_{\mathrm{gas}} + \frac{\partial\Omega_{\mathrm{arag}}}{\partial \mathrm{DIC}}\Delta\mathrm{DIC}_{\mathrm{Fw}} + \frac{\partial\Omega_{\mathrm{arag}}}{\partial \mathrm{Alk}}\Delta\mathrm{Alk}_{\mathrm{Fw}} + \frac{\partial\Omega_{\mathrm{arag}}}{\partial \mathrm{DIC}}\Delta\mathrm{DIC}_{\mathrm{Bio}} + \frac{\partial\Omega_{\mathrm{arag}}}{\partial \mathrm{Alk}}\Delta\mathrm{Alk}_{\mathrm{Bio}} + \frac{\partial\Omega_{\mathrm{arag}}}{\partial \mathrm{DIC}}\Delta\mathrm{DIC}_{\mathrm{Trans}} + \frac{\partial\Omega_{\mathrm{arag}}}{\partial \mathrm{Alk}}\Delta\mathrm{Alk}_{\mathrm{Trans}}, \quad (2)$$

where $\Delta\mathrm{DIC}_{\mathrm{gas}}$ is calculated by integrating annual CO_2 flux into the ocean. Similarly, ΔDIC_{Fw} and $\Delta\mathrm{Alk}_{\mathrm{Fw}}$ are obtained by integrating annual freshwater flux into the ocean, and $\Delta\mathrm{DIC}_{\mathrm{Bio}}$ and $\Delta\mathrm{Alk}_{\mathrm{Bio}}$ by integrating the terms relevant to carbon exchange in the ocean ecosystem model, such as phytoplankton respiration, phytoplankton photosynthesis, zooplankton excretion, detritus remineralization, and $CaCO_3$ formation. The first term on the right side of the equation in certain years is evaluated by the following equation:

$$\frac{\partial\Omega_{\mathrm{arag}}}{\partial T}\Delta T_{(\mathrm{yr})} \cong \{\Omega_{\mathrm{arag}}(T_{(\mathrm{yr})}, S_{(\mathrm{yr}-1)}, \mathrm{DIC}_{(\mathrm{yr}-1)}, \mathrm{Alk}_{(\mathrm{yr}-1)}) - \Omega_{\mathrm{arag}}(T_{(\mathrm{yr}-1)}, S_{(\mathrm{yr}-1)}, \mathrm{DIC}_{(\mathrm{yr}-1)}, \mathrm{Alk}_{(\mathrm{yr}-1)}) + \Omega_{\mathrm{arag}}(T_{(\mathrm{yr})}, S_{(\mathrm{yr})}, \mathrm{DIC}_{(\mathrm{yr})}, \mathrm{Alk}_{(\mathrm{yr})}) - \Omega_{\mathrm{arag}}(T_{(\mathrm{yr}-1)}, S_{(\mathrm{yr})}, \mathrm{DIC}_{(\mathrm{yr})}, \mathrm{Alk}_{(\mathrm{yr})})\} \times \frac{1}{2}, \quad (3)$$

where subscript yr denotes the target year. All of the terms except the transport term are evaluated in a similar manner. The transport term is calculated as the residual. pH also is divided into six components in a way similar to Ω_{arag}. The contribution of these components to Ω_{arag} and pH for the two model versions is integrated from 1850 to 2045 ($CO_2 \approx 520$ ppm, where the differences in pH and Ω_{arag} between the two model versions reach a maximum) to identify the main factors responsible for reducing pH and Ω_{arag} with rapid sea-ice reduction (Fig. 6). The terms are calculated for the uppermost 50 m. Gas exchange and transport terms are plotted together as "storage" because they nearly cancel each other.

Ω_{arag} for the Arctic Ocean decreases due to CO_2 uptake by gas exchange and dilution by freshwater input, and increases due to biological activity, seawater warming, freshening, and transport of carbon out of the top 50 m by lateral and vertical seawater

BGD
8, 10617–10644, 2011

exchanges. In OV, more than 85 % of the total reduction in Ω_{arag} (−0.55) is due to the storage effect of anthropogenic carbon (i.e. the sum of gas exchange (−1.12) and transport (0.65)); the freshwater effect (0.09) contributes less than 15 %. The rapid sea-ice reduction serves mainly to enhance effects of gas exchange, freshwater input, and biological activity. In NV, the sum of gas exchange and transport mainly causes a total reduction in Ω_{arag} (≈80 %), and the contribution of freshwater input to the reduction of Ω_{arag} is increased to ca. 20 %. Rapid sea-ice reduction decreases the effect of anthropogenic carbon storage by 0.13 (from −0.55 to −0.68) and that of freshwater input by 0.085 (from −0.09 to −0.175). Therefore, the analysis suggests that rapid sea-ice reduction decreases Ω_{arag} by an increase in both storage of anthropogenic carbon by gas exchange and freshwater input. The decreases in Ω_{arag} through freshwater input and the storage of anthropogenic carbon in the top 50 m due to rapid sea-ice reduction are partly (≈30 %) canceled out by the increase in biological productions. For the change in pH, seawater warming reduces pH, and the other five factors affect pH as they do Ω_{arag}. The reduction in pH with rapid sea-ice reduction also is caused by increased storage of anthropogenic carbon due to CO_2 uptake and freshwater input.

4.2 Different responses of pH and Ω_{arag} to high atmospheric CO_2 concentration

As shown in Sect. 3.3, the difference in pH in the Arctic surface waters between the two versions stays approximately 0.05 at CO_2 concentrations greater than 600 ppm, corresponding to the difference in seawater pCO_2 of 50 µatm, whereas that in Ω_{arag} almost disappears (Fig. 4). This different behavior is caused by the difference in dependence of these two parameters on seawater pCO_2 (Fig. 7). Since pH decreases almost linearly with increasing pCO_2, the difference in pCO_2 is directly reflected in pH throughout the simulation. While Ω_{arag} also decreases with an increase in pCO_2, the dependence of Ω_{arag} on pCO_2 weakens as pCO_2 increases. Therefore, the gap in predicted pCO_2 due to the difference of sea-ice extent under at CO_2 level near 600 ppm affects projections of Ω_{arag} and pH, while differences in the values at CO_2 levels grater than 600 ppm affects only pH. Summer and winter sea-ice reductions in NV occur more

BGD
8, 10617–10644, 2011

rapidly than in OV (Fig. 1). Annual CO_2 uptake in NV is, below CO_2 level of 600 ppm (≈2060 yr), dominated by summer air-sea gas exchange due to rapid summer sea-ice reduction, and at CO_2 levels greater than 650 ppm (≈2065 yr), due to winter sea ice reduction and the low sea surface temperature. In the comparison of the two model versions, the rapid decrease of Ω_{arag} in NV is caused basically by summer sea-ice reduction, while that of pH is caused by summer and winter sea-ice reduction.

4.3 The relationship between seasonal cycle of Ω_{arag} and sea-ice reduction

The seasonal cycle of surface Ω_{arag} in the Arctic Ocean also is affected by sea-ice reduction in the models (Fig. 8). In the Arctic surface waters, summer (winter) Ω_{arag} for the decade 1990–1999 in the two versions is lowest (highest) all the year round and the amplitude of seasonal variability is less than 0.1, which is consistent with the results reported by Steinacher et al. (2009). This seasonal cycle of Ω_{arag} is driven mainly by air-sea CO_2 exchange and freshwater input. The increases in CO_2 uptake and freshwater input due to summer sea-ice reduction reduced Ω_{arag}. The contributions of seawater temperature and biological processes are minimal.

The sea-ice reduction decreases the seasonal amplitude of freshwater input. In contrast, the effects of seawater temperature and biological processes are enhanced during summer sea-ice free condition, which increase Ω_{arag}. Thus, the amplitude of seasonal variation in Ω_{arag} is decreased to 0.04 by the year 2060 (2090) in NV (OV). Further on, winter sea-ice reduction changes the seasonal cycle of air-sea gas exchange. After the year 2065 in NV, the Arctic surface waters absorb CO_2 in winter and release it in summer since CO_2 is more soluble in cold seawater. Thus, Ω_{arag} is decreased in winter due to an increase in CO_2 uptake and seawater cooling, whereas it is increased in the summer due to CO_2 release, seawater warming, and biological processes. The contribution of freshwater input is relatively small. In NV for the decade 2090–2099, summer (winter) Ω_{arag} is about 0.05 higher (lower) than the annual mean value. This change in seasonal cycle of Ω_{arag} is not found in OV in which reduction of sea-ice extent relative to the present day is only 30 % at about the year 2100.

BGD
8, 10617–10644, 2011

5 Conclusions

Impacts of sea-ice reduction on the future projection of pH and aragonite saturation values in the Arctic surface waters have been investigated by comparing the rates of ocean acidification calculated from outputs of two versions of an earth system model in which Summer Arctic ice-free condition by 2040 and 2090, respectively, is projected under similar CO_2 emission scenarios. Results indicated that the maximum differences in pH and Ω_{arag} between the two model versions are 0.08 and 0.15, respectively, at atmospheric CO_2 levels of 520 ppm (year $\approx$ 2045, a few years after the difference in summer sea-ice extent reaches a maximum). The critical atmospheric CO_2 concentration, at which the Arctic surface waters become undersaturated with respect to aragonite in annual mean, is reduced from 550 to 480 ppm due to rapid sea-ice reduction. In the classification of CO_2 stabilization scenarios by IPCC AR4, this decrease in critical CO_2 concentration corresponds to a shift from category IV to III (IPCC, 2007). The earlier emergence of undersaturated surface water due to rapid sea-ice reduction is a factor to be considered in determining CO_2 stabilization concentration.

The analysis showed that rapid sea-ice reduction decreases pH and aragonite saturation state due to increases in both CO_2 uptake by air-sea gas exchange and freshwater input from an increase in sea-ice meltwater. Comparison between the two model versions reveals that CO_2 uptake and freshwater input contributes at ratio of 3:2 to reduce aragonite saturation state due to rapid sea-ice reduction, and about 30 % of these contributions are canceled out by an increase in biological processes.

For the CO_2 concentration greater than 600 ppm, the difference in pH in the Arctic surface waters between the two model versions is maintained around 0.05, consistent with the difference in seawater pCO_2 of 50 µatm due to differences in sea-ice reduction, whereas the difference in Ω_{arag} values almost disappears. Thus, the difference in pCO_2 is directly reflected in pH throughout the simulation owing to a linear reduction in pH with pCO_2, while the dependence of Ω_{arag} reduction on pCO_2 weakens as pCO_2 increases. For the seasonal variability of Ω_{arag}, the summer sea-ice reduction weakens

BGD
8, 10617–10644, 2011

the seasonal amplitude because seasonal variability in freshwater input decreases, and that in seawater temperature and biological productions increases. Furthermore, the change in the seasonal cycle of CO_2 uptake due to winter sea-ice reduction reverses the seasonal cycle of Ω_{arag}.

Our results indicate that future projections of pH and aragonite saturation state in Arctic surface waters can be influenced significantly by the rapidity of sea ice reduction as well as by increases in atmospheric CO_2 concentrations. We emphasize that accurate modeling of sea-ice dynamics is crucial for projections related to not only global warming but also ocean acidification for the Arctic Ocean.

Acknowledgements. We thank Michiyo Yamamoto-Kawai and Fiona A. McLaughlin for providing the observation datasets for the Joint Ocean Ice Study (JOIS) 2008. This study was supported by the Innovative Program of Climate Change Projection for the 21st Century, MEXT, Japan. The numerical simulations in this study were performed using the Earth Simulator, and all the figures were produced with the GFD-DENNOU Library.

References

Bates, N. R., Mathis, J. T., and Cooper, L. W.: Ocean acidification and biologically induced seasonality of carbonate mineral saturation states in the western Arctic Ocean, J. Geophys. Res., 114, C11007, doi:10.1029/2008JC004862, 2009.

Friedlingstein, P., Cox, P., Betts, R., Bopp, L., Von Bloh, W., Brovkin, V., Cadule, P., Doney, S., Eby, M., Fung, I., Bala, G., John, J., Jones, C., Joos, F., Kato, T., Kawamiya, M., Knorr, W., Lindsay, K., Matthews, H. D., Raddatz, T., Rayner, P., Reick, C., Roeckner, E., Schnitzler, K. G., Schnur, R., Strassmann, K., Weaver, A. J., Yoshikawa, C., and Zheng, N.: Climate-Carbon Cycle Feedback Analysis: Results from the C^4MIP Model Inter-comparison: Evolution of carbon sinks in a changing climate, J. Climate, 19, 3337–3343, 2006.

Gangstø, R., Gehlen, M., Schneider, B., Bopp, L., Aumont, O., and Joos, F.: Modeling the marine aragonite cycle: changes under rising carbon dioxide and its role in shallow water $CaCO_3$ dissolution, Biogeosciences, 5, 1057–1072, doi:10.5194/bg-5-1057-2008, 2008.

Holland, M. M., Bitz, C. M., and Tremblay, B.: Future abrupt reductions in the summer Arctic sea ice, Geophys. Res. Lett., 33, L23503, doi:10.1029/2006GL028024, 2006.

BGD
8, 10617–10644, 2011

Hunke, E. and Dukowicz, J. K.: An elastic-viscous-plastic model for sea ice dynamics, J. Phys. Oceanogr., 27, 1849–1867, 1997.

Intergovernmental Panel on Climate Change (IPCC): Climate Change 2007: The Physical Science Basis, in: Contribution of Working Group I to the Fourth Assessment Report of the Intergovernmental Panel on Climate Change, edited by: Solomon, S., Qin, D., Manning, M., Chen Z., Marquis, M., Averyt, K. B., Tignor, M., and Miller, H. L., Cambridge Univ. Press, Cambridge, UK, 996 pp., 2007.

Ishimatsu, A., Hayashi, M., Lee K.-S., Kikkawa, T., and Kita. J.: Physiological effects on fishes in a high-CO2 world, J. Geophys. Res., 110, C09S09, doi:10.1029/2004JC002564, 2005.

Ito, A. and Oikawa, T.: A simulation model of the carbon cycle in land ecosystems Sim-CYCLE: A description based on dry-matter production theory and plot-scale validation, Ecol. Modell., 151, 147–179, 2002.

K-1 Model Developers: K-1 Coupled GCM (MIROC) description, K-1 Tech. Rep. 1, Cent. for Clim. Syst. Res. (Univ. of Tokyo), Natl. Inst. for Environ. Stud., and Frontier Res. Cent. for Global Change, Yokohama, Japan, available at http://www.ccsr.u-tokyo.ac.jp/kyosei/hasumi/MIROC/tech-repo.pdf, 2004.

Kawamiya, M., Kishi, M. J., and Suginohara, N.: An ecosystem model for the North Pacific embedded in a general circulation model Part II: Mechanisms forming seasonal variations of chlorophyll, J. Marine Systems, 25, 159–178, 2000.

Kawamiya, M., Yoshikawa, C., Kato, T., Sato, H., Sudo, K., Watanabe, S., and Matsuno, T.: Development of an integrated Earth system model on the earth simulator, J. Earth Simulator, 4, 18–30, available at http://www.jamstec.go.jp/esc/publication/journal/jes_vol.4/index.html, 2005.

Locarnini, R. A., Mishonov, A. V., Antonov, J. I., Boyer, T. P., and Garcia, H. E.: World Ocean Atlas 2005, vol. 1, Temperature, NOAA Atlas NESDIS 61, edited by: Levitus, S., US Govt. Print. Off., Washington, D.C., 2006.

Marland, G., Boden, T. A., and Andres, R. J.: Global, regional, and national CO_2 emissions. Trends: A compendium of data on global change. Carbon Dioxide Inf. Anal. Cent., Oak Ridge Natl. Lab, US Dep. of Energy, Oak Ridge, Tenn., 2005.

McNeil, B. I. and Matear, R. J.: Southern ocean acidification: a tipping point at 450-ppm atmospheric CO_2, Proceedings of the National Academy of Sciences, 105, 18860–18864, 2008.

Millero, F. J.: Thermodynamics of the carbon dioxide system in the oceans, Geochim. Cosmochim. Ac., 59, 661–677, 1995.

BGD
8, 10617–10644, 2011

Mucci, A.: The solubility of calcite and aragonite in seawater at various salinities, temperatures and 1 atmosphere total pressure, Am. J. Sci., 238, 780–799, 1983.
Orr, J. C., Najjar, R., Sabine, C. L., and Joos, F.: Abiotic-HOWTO, internal OCMIP report, 25 pp., LSCE/CEA Saclay, Gif-sur-Yvette, France, 1999.
Orr, J. C., Fabry, V. J., Aumont, O., Bopp, L., Doney, S. C., Feely, R. A., Gnanadesikan, A., Gruber, N., Ishida, A., Joos, F., Key, R. M., Lindsay, K., Maier-Reimer, E., Matear, R., Monfray, P., Mouchet, A., Najjar, R. G., Plattner, G.-K., Rodgers, K. B., Sabine, C. L., Sarmiento, J. L., Schlitzer, R., Slater, R. D., Totterdell, I. J., Weirig, M. F., Yamanaka, Y., and Yool, A.: Anthropogenic ocean acidification over the twenty-first century and its impact on calcifying organisms, Nature, 437, 681–686, 2005.
Oschlies, A.: Model-derived estimates of new production: New results point towards lower values, Deep Sea Res. Part II, 48, 2173–2197, 2001.
Oschlies, A. and Garcon, V.: An eddy-permitting coupled physicalbiological model of the North Atlantic 1. Sensitivity to advection numerics and mixed layer physics, Global Biogeochem. Cycles, 13, 135–160, 1999.
Royal Society: Ocean acidification due to increasing atmospheric carbon dioxide, The Royal society, London, 223 pp., 2005.
Sabine, C. L., Feely, R. A., Gruber, N., Key, R. M., Lee, K., Bullister, J. L., Wanninkhof, R., Wong, C. S., Wallace, D. W. R., Tilbrook, B., Milllero, F. J., Peng, T.-H., Kozyr, A., Ono, T., and Rios, A. F.: The Oceanic Sink for Anthropogenic CO_2, Science, 305, 367–371, 2004.
Sato, H., Itoh, A., and Kohyama, T.: SEIB-DGVM: A new dynamic global vegetation model using a spatially explicit individual-based approach, Ecological Modelling, 200, 279–307, doi:10.1016/j.ecolmodel.2006.09.006, 2007.
Seibel, B. A. and Walsh, P. J.: Potential impacts of CO2 injections on deep-sea biota, Science, 294, 319–320, 2001.
Semtner Jr., A. J.: A model for the thermodynamic growth of sea ice in numerical investigations of climate, J. Phys. Oceanogr., 6, 379–389, 1976.
Steinacher, M., Joos, F., Frlicher, T. L., Plattner, G.-K., and Doney, S. C.: Imminent ocean acidification in the Arctic projected with the NCAR global coupled carbon cycle-climate model, Biogeosciences, 6, 515–533, doi:10.5194/bg-6-515-2009, 2009.
Stroeve, J., Holland, M. M., Meier, W., Scambos, T., and Serreze, M.: Arctic sea ice decline: Faster than forecast, Geophys. Res. Lett., 34, L09501, doi:10.1029/2007GL029703, 2007.
Wang, M. and Overland, J. E.: A sea ice free summer Arctic within 30 years?, Geophys. Res.

BGD
8, 10617–10644, 2011

Lett., 36, L07502, doi:10.1029/2009GL037820, 2009.
Watanabe, S., Hajima, T., Sudo, K., Nagashima, T., Takemura, T., Okajima, H., Nozawa, T., Kawase, H., Abe, M., Yokohata, T., Ise, T., Sato, H., Kato, E., Takata, K., Emori, S., and Kawamiya, M.: MIROC-ESM 2010: model description and basic results of CMIP5-20c3m experiments, Geosci. Model Dev., 4, 845–872, doi:10.5194/gmd-4-845-2011, 2011.
Yamamoto-Kawai, M., McLaughlin, F. A., Carmack, E. C., Nishino S., and Shimada, K.: Aragonite Undersaturation in the Arctic Ocean: Effects of ocean acidification and sea ice melt, Science, 326, 1098–1100, doi:10.1126/science.1174190, 2009.
Yoshikawa, C., Kawamiya, M., Kato, T., Yamanaka, Y., and Matsuno, T.: Geographical distribution of the feedback between future climate change and the carbon cycle, J. Geophys. Res., 113, G03002, doi:10.1029/2007JG000570, 2008.
Zeebe, R. E., Zachos, J. C., Caldeira, K., and Tyrrell, T.: Carbon emissions and acidification, Science, 321, 51–52, 2008.

BGD
8, 10617–10644, 2011

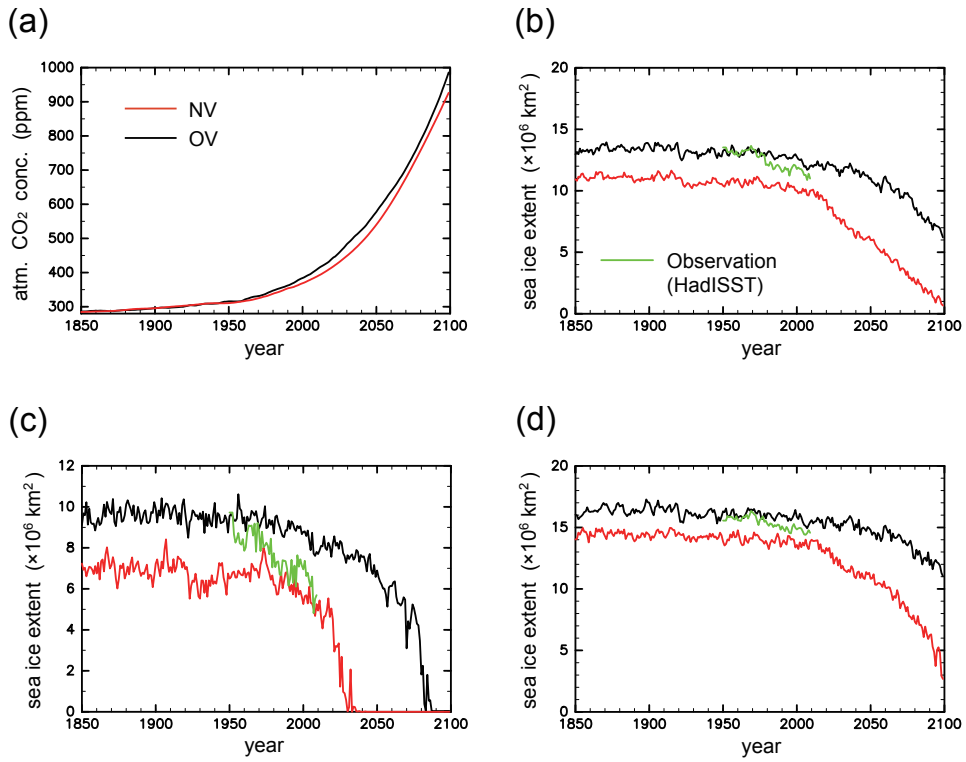

Fig. 1. Projected global annual mean atmospheric CO_2 concentrations **(a)**. Annual mean **(b)**; September mean **(c)**; March mean; and **(d)** sea-ice extent in the Arctic Ocean for old (black) and new (red) model versions. The green line is based on HadISST analysis.

BGD
8, 10617–10644, 2011

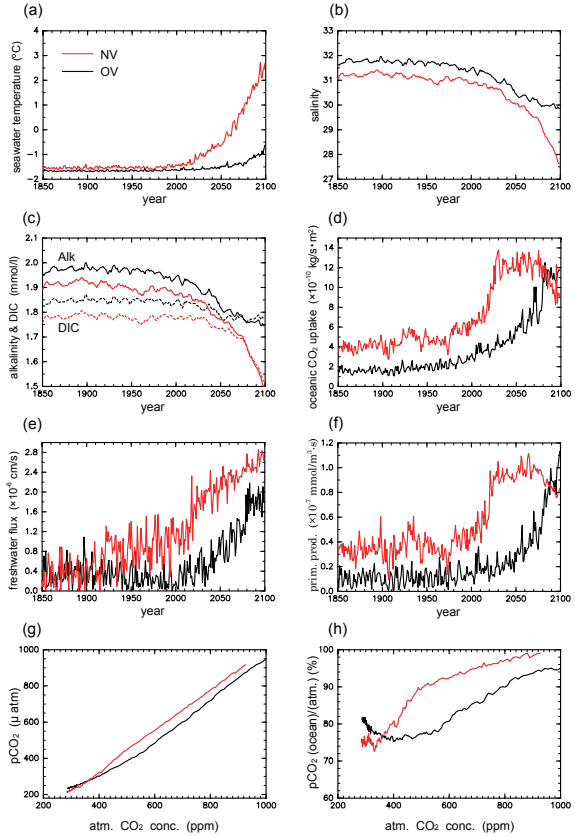

Fig. 2. **(a)** Observation sites of ODEN-91, AOS-94, and ARCSYS-96 (black open circle), and JOIS 2008 (red open circle). The vertical distribution of Ω_{arag} calculated from **(b)** ODEN-91, AOS-94, and ARCSYS-96; and **(c)** JOIS 2008. The dots represent raw data and lines represent horizontal average. Red and blue show Ω_{arag} calculated from old and new model versions for the same time and place.

BGD
8, 10617–10644, 2011

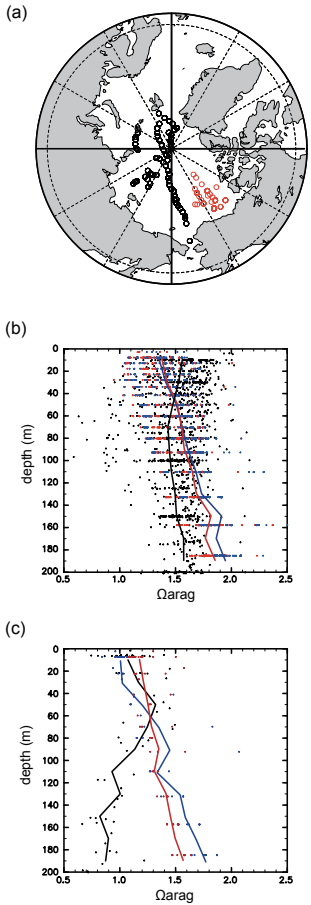

Fig. 3. Calculated annual mean: **(a)** seawater temperature; **(b)** salinity; **(c)** alkalinity and DIC; **(d)** oceanic CO_2 uptake; **(e)** freshwater input; **(f)** primary production; **(g)** seawater pCO_2; and **(h)** fraction of pCO_2 between ocean and atmosphere at the Arctic surface for old (black) and new (red) model versions.

BGD
8, 10617–10644, 2011

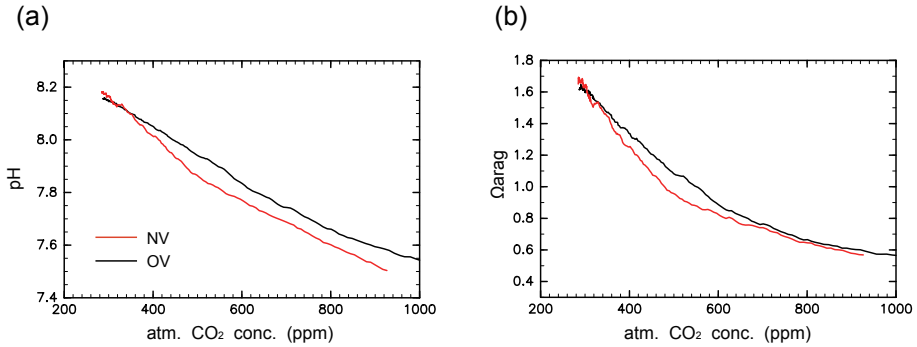

Fig. 4. Change in modified annual mean of **(a)** pH and **(b)** Ω_{arag} with atmospheric CO_2 concentration in the Arctic surface waters for old (black) and new (red) model versions.

BGD
8, 10617–10644, 2011

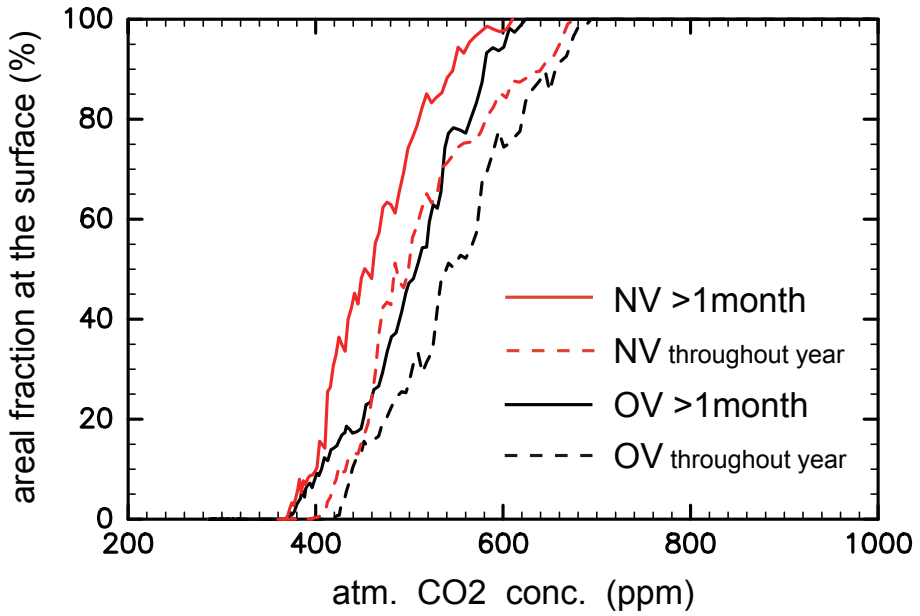

Fig. 5. The evolution of the areal fraction of undersaturated surface water with atmospheric CO_2 concentration for old (black) and new (red) model versions. The solid and dashed lines represent evolution in at least one month of the year and throughout year, respectively.

BGD
8, 10617–10644, 2011

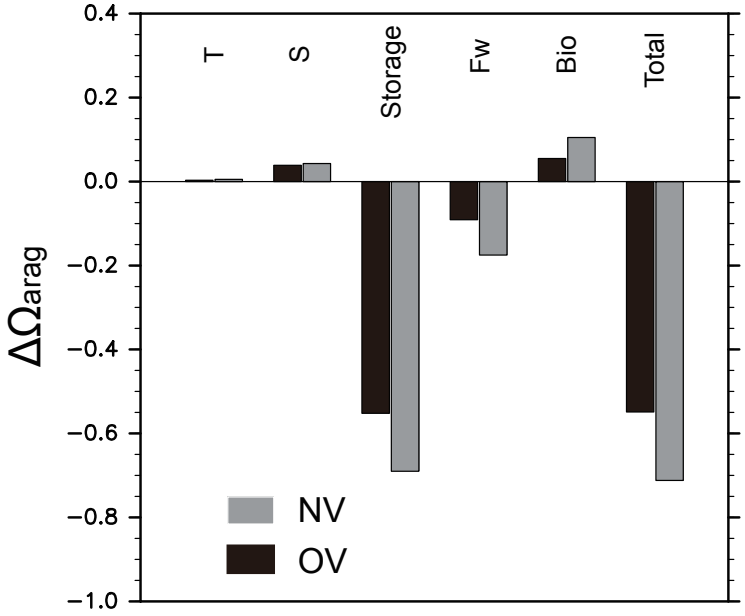

Fig. 6. Projected changes in the annual mean difference Ω_{arag} from 1850 to 2045 ($CO_2 \approx$ 520 ppm) in the top 50 m of the Arctic Ocean for old (black) and new (gray) model versions. The total change is divided into contributions by changes in seawater temperature (T), salinity (S), CO_2 uptake by gas exchange (Gas), freshwater input (Fw), biology (Bio) and transport of carbon by lateral and vertical seawater exchange (Trans). For the gas exchange and transport terms, only the sum of the two (defined as "storage") is plotted.

BGD
8, 10617–10644, 2011

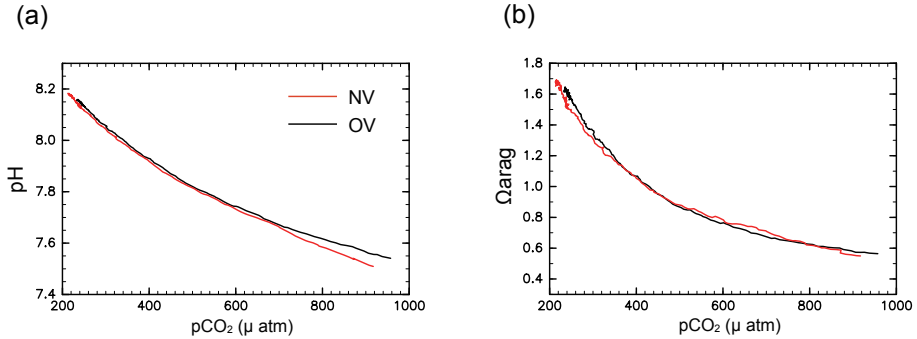

Fig. 7. Calculated annual mean **(a)** pH and **(b)** Ω_{arag} with seawater pCO_2 in the Arctic surface waters for old (black) and new (red) model versions.

BGD
8, 10617–10644, 2011

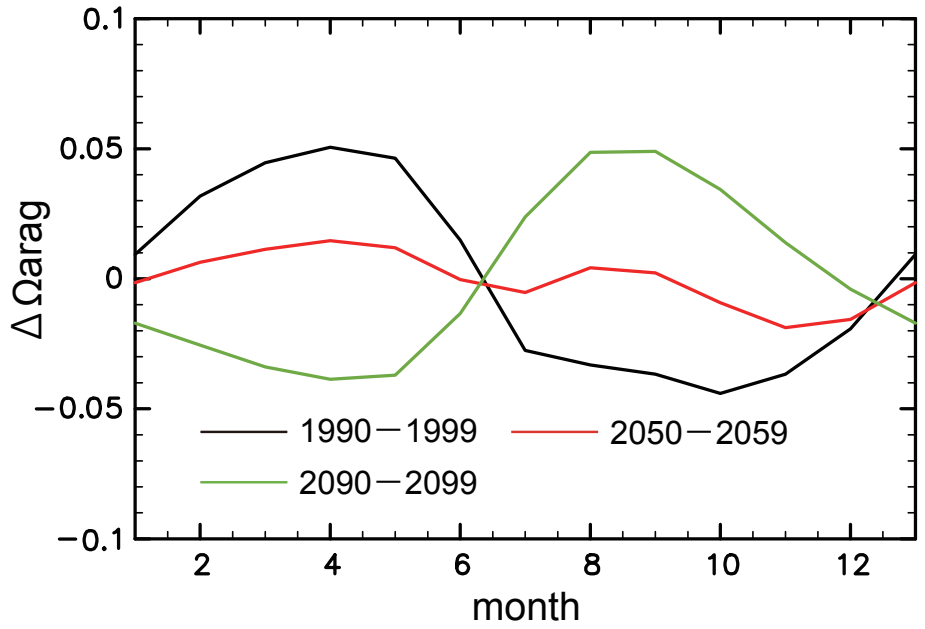

Fig. 8. Calculated seasonal deviation in Ω_{arag} in the Arctic Ocean in NV from the annual mean for 1990–1999 (black), 2050–2059 (red), and 2090–2099 (green).

BGD
8, 10617–10644, 2011